JBC Papers in Press. Published on April 26, 2016 as Manuscript M115.709659
The latest version is at http://www.jbc.org/cgi/doi/10.1074/jbc.M115.709659

Rearrangement of the extracellular domain/extracellular loop 1 interface is critical for thyrotropin receptor activation

Joerg Schaarschmidt[1,a], Marcus B. M. Nagel[1,a,b], Sandra Huth[a], Holger Jaeschke[a], Rocco Moretti[c], Vera Hintze[d], Martin von Bergen[b,e,f], Stefan Kalkhof[b,g], Jens Meiler[c], and Ralf Paschke[h]

From the [a]Department of Internal Medicine, University of Leipzig, 04103 Leipzig, Germany, [b]Department of Proteomics, Helmholtz-Centre for Environmental Research, 04318 Leipzig, Germany, [c]Department of Chemistry and Center for Structural Biology, Vanderbilt University, Nashville, TN 37235, United States of America, [d]Institute of Materials Science, Max Bergmann Center of Biomaterials, TU Dresden, 01069 Dresden, Germany, [e]Faculty of Biosciences, Pharmacy and Psychology, Institute of Biochemistry, University Leipzig, Leipzig, Germany, [f]Aalborg University, Department of Chemistry and Bioscience, Fredrik Bajers Vej 7, 9220 Aalborg, Denmark, [g]Department of Bioanalytics, University of Applied Sciences and Arts of Coburg, 96450 Coburg, Germany, [h]Division of Endocrinology and Metabolism & Arnie Charbonneau Cancer Institute University of Calgary, Calgary, AB T2N 1N4, Canada

Running title: Full-length TSHR models

Keywords: cell signaling computer modeling, G protein-coupled receptor (GPCR), mass spectrometry (MS), protein cross-linking, receptor structure-function, site-directed mutagenesis, structural biology, surface plasmon resonance (SPR)

To whom correspondence should be addressed: Prof. Dr. Ralf Paschke, Richmond Road Diagnosis and Treatment Centre (RRDTC), University of Calgary, 1820 Richmond RD SW, Calgary AB T2T5C7, Telephone: (403) 955 8969, FAX: (403) 955 8248, E-Mail: ralf.paschke@ucalgary.ca

ABSTRACT

The thyroid stimulating hormone receptor (TSHR) is a G protein-coupled receptor (GPCR) with a characteristic large extracellular domain (ECD). TSHR activation is initiated by binding of the hormone ligand TSH to the ECD. How the extracellular binding event triggers the conformational changes in the transmembrane domain (TMD) necessary for intracellular G protein activation is poorly understood. To gain insight in this process, the knowledge on the relative positioning of ECD and TMD and the conformation of the linker region at the interface of ECD and TMD are of particular importance. To generate a structural model for the TSHR we applied an integrated structural biology approach combining computational techniques with experimental data. Chemical crosslinking followed by mass spectrometry (XL-MS) yielded 17 unique distance restraints within the ECD of the TSHR, its ligand TSH and the hormone/receptor complex. These structural restraints generally confirm the expected binding mode of TSH to the ECD as well as the general fold of the domains and were used to guide homology modelling of the ECD. Functional characterization of TSHR mutants confirms the previously suggested close proximity of S281 and I486 within the TSHR. Rigidifying this contact permanently with a disulfide bridge disrupts ligand-induced receptor activation and indicates that rearrangement of the ECD/extra-cellular loop (ECL) 1 interface is a critical step in receptor activation. The experimentally verified contact of S281 (ECD) and I486 (TMD) was subsequently utilized in docking homology models of the ECD and the TMD to create a full-length model of a GPHR.

INTRODUCTION

Glycoprotein hormones (GPHs) normally regulate crucial processes in metabolism and reproduction by activating GPHRs. This is especially true for TSHR, which can cause several clinically relevant conditions like hypo- and hyperthyroidism when it malfunctions. Yet the mechanism of how extracellular ligand binding

[1] contributed equally

Copyright 2016 by The American Society for Biochemistry and Molecular Biology, Inc.

Downloaded from http://www.jbc.org/ at Vanderbilt University - Biomedical & Science/Engineering Libraries on November 7, 2016

induces the structural changes required for intracellular G-protein activation is unknown. We pursued an integrated structural biology approach using modelling guided by experimental data to generate experimentally supported full-length TSHR models. It is expected that some insights gleaned from a TSHR model can be generalized to other GPHRs. These models in turn create testable hypotheses on the mechanism of GPHR activation and can promote drug development to treat GPHR associated diseases.

GPHs bind to the ECD of their respective receptors (Fig. 1A) and consequently initiate activation, which is presumably propagated by induction of conformational changes within the ECD's hinge region (HR) (1-4). Interestingly, GPHRs still possess a binding site within the TMD not associated with physiological receptor activation but accessible to low-molecular-weight agonists and allosteric modulators (5-7). Another important aspect of GPHR function and physiology is posttranslational modification, including disulfide bond formation, glycosylation, tyrosine sulfation and proteolytic cleavage with the latter only occurring during maturation of the TSHR (reviewed by Kursawe *et al.* (8)). However there is no evident physiological requirement for proteolytic excision of the approximately 50 amino acid C-peptide, with a deletion variant showing similar characteristics to the wild type (wt) receptor (9). In contrast, glycosylation and sulfation are obligatory with the latter being an indispensable feature of specific hormone binding (8, 10). The structure of the ECD of the follicle stimulating hormone receptor (FSHR, a member of the GPH subfamily) in complex with FSH (11) showed that the ECD forms a continuous hand-shaped structure. In this the C-terminal HR does not form a separate structural entity as previously anticipated but rather comprises the last two β-sheets of the LRR-fold, an α-helix as well as the "thumb" region including the sulfation located at the interface to the hormone. Despite these invaluable insights on ligand binding and specificity, many details about GPHR activation are still elusive. These include the potential role of the HR residues with unresolved electron density, the significance of receptor oligomerization, and negative cooperativity in hormone binding (4). A major obstacle in understanding GPHR activation has been the lack of an atomic detail model, particularly one that defines the relative orientation of ECD and TMD, identifies interacting residues at the interface, and illustrates the structural changes upon ligand binding within the HR and the interface.

In pursuit of a full-length structural GPHR model we implement an integrated computational/experimental approach. Chemical cross-linkers (XL) of a defined maximal length react intra- or inter-molecularly with two functional groups on the protein surface. After enzymatic digestion, the resulting fragments are identified by mass spectrometry (MS). Based on the spacer lengths an approximate upper boundary for the distance is derived and employed as restraint for the structural models (12). This approach is limited to the soluble ECD because of difficulties purifying a functional, full-length TSHR, even in the very low quantities needed for crosslinking experiments (11, 13). Therefore, we additionally use double-mutant cycle analysis and disulfide cross-linking to assess the direct contact between amino acids at the ECD/TMD interface (14, 15). Even though resulting structural restraints are sparse, they are sufficient to build structural models for the full-length TSHR with the Rosetta software suite (16). These models provide insights to TSHR activation. Specifically, we predict the relative orientation of ECD and TMD, potentially important contact points at the ECD/TMD interface, and the conformational changes necessary for receptor activation. The high sequence conservation of the investigated region within the GPHR subfamily, as well as studies on chimeric receptors (17, 18), suggest a shared activation mechanism with receptor-specific interactions. The reported approach can therefore be expanded to the remaining GPHRs and provide new insights into similarities as well as receptor-specific features of GPHR activation.

EXPERIMENTAL PROCEDURES

Purification of the soluble TSHR-ECD

A soluble TSHR-ECD with a 10 Histidine Tag and a GPI Anchor (TSHR_ECD10HisGPI) was expressed and purified as previously described (13). Briefly, the gene was stably transfected into CHO Flp-In™ cells (Thermo Fisher Scientific, Waltham, MA) according to the manufacturer's instructions. Purification was performed by liquid chromatography at 4°C with a Ni-Sepharose high-

Downloaded from http://www.jbc.org/ at Vanderbilt University - Biomedical & Science/Engineering Libraries on November 7, 2016

performance affinity column (HisTrap HP 5 ml, GE Healthcare). After column equilibration the sample was applied (flow rate: 0.5 ml/min) and the collected fractions were tested for presence and purity of the soluble ECD by SDS-PAGE followed by Coomassie staining or Western blotting with Anti-TSH Receptor antibody (A9, abcam®). Fractions containing the ECD in sufficient quantity and purity (>70%) were combined, concentrated and buffer exchanged with PBS with a centrifugal concentrator (Corning® Spin-X® UF 20mL, MWCO 10 kDa).

Cell culture, transient expression and characterization of wild type and mutant full-length – TSHR

Mutations were introduced into the hTSHR gene, tagged with an N-terminal hemagglutinin (HA)-tag, in a pcDNA3.1(-)/hygromycin vector via site-directed mutagenesis, as described previously (6). COS-7 Cells were then transiently transfected with the wild type (wt) and mutated vectors using the GeneJammer transfection reagent (Stratagene, Amsterdam, NL). Functionality of expressed TSHR variants was evaluated, as described previously (19, 20), by determining cell surface expression, specific binding of bovine TSH (bTSH, National Hormone and Pituitary Program of the National Institute of Diabetes and Digestive and Kidney Diseases), basal and bTSH (30 mU) induced cAMP accumulation, and linear regression analysis (LRA) of basal cAMP accumulation versus cell surface expression.

The Gq/11 activation was determined in HEK_{GT}-cells by cotransfection of the vectors with a reporter vector harboring the firefly luciferase gene under the control of the nuclear factor of activated T-cells (NFAT) transcription factor (pNFAT-Luc, Agilent Technologies, Santa Clara, CA). 48 h after transfection cells were stimulated for 4 h with bTSH (30 mU) and lysed with Luciferase Cell Culture Lysis Reagent (Promega, Madison, WI). Luciferase activity was determined as described previously by Hampf *et al.* (21).

MS analysis of crosslinked soluble TSHR-ECD

Chemical crosslinking of the soluble TSHR-ECD with bTSH was performed as previously described (12, 22) with disuccinimidyl tartrate (DST), bis(sulfosuccinimidyl) suberate-D0/D4 (BS3), ethylene glycol bis(sulfosuccinimidylsuccinate) (sulfo-EGS), and PEGylated bis(sulfosuccinimidyl)suberate (BS(PEG)5) obtained from Thermo Fisher Scientific Inc. (Rockford, IL, USA), as well as BS3-D0/D12 obtained from Creative Molecules Inc. (Toronto, OLN, Canada). All cross-linking reactions were conducted in 1X PBS buffer, pH 7.2 at a protein concentration of 3.3 or 2.5 µM. The molar ratio of protein to cross-linker was 1:100 or 1:200, respectively, and the reaction was quenched after 60 and 120 min with ammonium bicarbonate buffer equimolar to the cross-linkinging reagent. The cross-linking reagents BS3 and sulfo-EGS were resolved in 1X PBS at a final concentration of 0.1 mol/l. Hydrophobic cross-linking reagents $BS(PEG)_5$ and DST were freshly prepared in dry DMSO to a final concentration of 0.25 mol/l and 0.1 mol/l respectively.

The crosslinked proteins were deglycosylated with 250 U of PNGase F according to the manufacturer's instructions. The samples were subsequently separated by gradient SDS-PAGE (4-12%). Bands at the positions corresponding to molecular weight of TSHR-ECD, TSH and the complex were excised and samples were reduced, alkylated and digested in-gel using trypsin.

The resulting peptide mixtures were analyzed by nano-HPLC/nano-ESI-MS/MS using either an Orbitrap Fusion Tribrid or LTQ Orbitrap XL ETD mass spectrometer. Identification was performed using the software StavroX (23), allowing a mass deviation of 15 ppm (LTQ Orbitrap) or 10 ppm (Orbitrap Fusion) for MS precursors and 0.5 Da (collision induced dissociation, LTQ Orbitrap XL ETD) or 0.1 Da (higher-energy collisional dissociation, Orbitrap Fusion Tribrid) for fragment ions.

Surface Plasmon Resonance

Surface plasmon resonance was performed on a T100 (Biacore, Uppsalare, UC, Sweden). Recombinant TSHR-ECD was amine-coupled on a CM3-Chip following standard procedures. The final protein loaded amounted to 210 RU. Experiments were conducted for eight different ligand concentrations (1500, 500, 166.67, 55.56, 18.52, 6.17, 2.06 and 0 nM) at a flow rate of 30 µl/min and 25 °C. Contact time of the ligand was 300 s followed by 800 s dissociation time. The regeneration was performed using 2.5 M NaCl in HBS-EP for 30 s followed by 200 s for stabilization.

Downloaded from http://www.jbc.org/ at Vanderbilt University - Biomedical & Science/Engineering Libraries on November 7, 2016

Data analysis was performed using Sigma Plot 12.0 (Systat Software Inc, Bangalore, Karnataka, India) and Biacore T100 evaluation Software 2.03.

Nano-HPLC/nanoESI-LTQ Orbitrap XL ETD MS

Samples were prepared in 0.1 % FA, injected in a NanoAcquidity UPLC, trapped and desalted for 10 min on a C_{18} trapping column (nanoACQUITY symmetry trapping coloumn, Waters) with a constant flow of 15 µl/min and 2% ACN. After 8 min the peptides were eluted and separated on a C_{18} reverse phased column (ACQUITY UPLC Peptide BEH C18 nanoACQUITY, Waters) using a linear ACN gradient (8-45%) over 85 min or 140 min (Waters Corporation, Milford, MA, USA) at a flow rate of 300 nl/min. The HPLC-systems was coupled online to a mass spectrometer via a chip based nano ESI source (TriVersa NanoMate, Advion, Ithaca, NY, USA). The spray voltage was set to 1.6-1.8 kV and the capillary was heated to 250°C. MS/MS-scans were triggered automatically after each full scan (*m/z* range of 400-2000, resolution of 60.000, 1 microscan and $5x10^5$ ions accumulated) for the 6 or 10 highest abundant precursor ions, exceeding an intensity of 10^3 and charge state ≥2. The employed lock mass for online recalibration was 445.1200 m/z. Further the instrument was set to exclude ions from a dynamic exclusion list (500 entries) with a maximal retention period of 60 s and a relative mass window of ±3 Da for MS/MS scans. Fragmentation of selected precursor ions ±4 Da was caused by collision induced dissociation (CID) with ramped normalized collision energy of 37±15 (three steps). Activation Energy (Q) was set to 0.250 with an activation time of 30 ms. The AGC target was set to 8000 ions and the fragment analysis took place in the ion trap.

Nano-HPLC/ nanoESI- Orbitrap Fusion Tribrid MS

Samples were prepared in 0.1 % FA, injected in an UltiMate 300 HPLC, trapped and desalted for 8 min on a C_{18} column (Acclaim PepMap100) with a constant flow of 5 µl/min and 2 % ACN. Afterwards peptides were eluted and separated on a C_{18} separation column (Acclaim PepMap RSLC coloumn) using a linear ACN gradient (8-45 %) over 80 or 130 min (Dionex Corporation, Sunnyvale, CA, USA) at a flow rate of 300 nl/min. The HPLC-systems was coupled online to a mass spectrometer via a chip based nano ESI source (TriVersa NanoMate, Advion). The spray voltage was set to 1.7-1.8 kV and the capillary was heated to 275 °C. MS/MS-scans were triggered automatically after each full scan (m/z range of 350-2000, a resolution of 60.000, 1 microscan and $5x10^5$ ions accumulated) using a top speed decision tree (5 s cycle time) setting the highest priority for the highest charge state, followed by the highest abundance. Precursor ion intensity was required to exceed $2x10^3$ and the charge state was restricted to a range of 2-7 m/z. The employed lock mass was 445.1200 m/z. The instrument was set to exclude ions from a dynamic exclusion list with a maximal retention period of 15 s and a relative mass window of ± 20 ppm for MS/MS scans. Fragmentation of selected precursor ions ±4 Da was caused by higher-energy collisional dissociation (HCD) with stepped normalized collision energy of 35±10. The AGC target was set to 5.000 ions. Fragment ions were detected in the Orbitrap at a resolution of 15.000.

Molecular modeling of the full-length TSHR

The homology model of the TSHR-ECD in complex with bovine TSH was generated using Rosetta 3 (16, 24). Briefly, homology modeling was based on the structure of the FSHR-ECD in complex with FSH ((11); PDB-ID: 4ay9). In addition, sections of the LRR domain were replaced by the coordinates of the TSHR-LRR domain ((25); PDB-ID 2xwt) after superimposing the residues at the junctions (cut after L57 or S234 of the TSHR-LRR domain). The protein sequences of the TSHR-ECD and TSH were subsequently aligned to the structural coordinates of the template structures. For each template a set of 2000 models (150 for the FSHR template) was built, reconstructing backbone coordinates in gapped regions of the alignment using the cyclic coordinate descent (CCD) protocol followed by a relaxation of the structures after side chain coordinates were added from a rotamer library. The structures were clustered using Calibur (26). In addition Cβ-distances for each model were determined with Rosetta's contactMap protocol (20).

Homology models of the TSHR-TMD were generated with the RosettaCM protocol as described by Song *et al.* (27). Homology modelling was performed for 20 templates of class A GPCRs considered to be in an inactive conformation (4n6h, 2rh1, 3uon, 4ej4, 4eiy, 1u19, 3rze, 4bvn, 4dkl,

Downloaded from http://www.jbc.org/ at Vanderbilt University - Biomedical & Science/Engineering Libraries on November 7, 2016

2z73, 4u15, 4djh, 4ea3, 3v2y, 4mbs, 4ib4, 3pbl, 4ntj, 3odu) and 7 templates considered to be in an active conformation (4lde, 4mqs, 2ydv, 4j4q, 2y00, 3ayn, 4iar). A sequence and structure based alignment of the templates was performed with the Molecular Operating Environment (MOE, 2012.10; Chemical Computing Group Inc., Montreal, QC, Canada) with manual adjustment of the alignment removing gaps within the core TM regions. For each template set 5000 models were generated and the resulting models were clustered with Calibur, both as separate sets and combined.

All homology models were evaluated based on energy and cluster size. The best scoring model from each of the 5 largest ECD model clusters was subsequently docked to the three best scoring models from each of the 10 largest TM domain clusters. Prior to the docking run the C-terminal loop segment of the ECD, which most likely adopts an unrepresentative conformation in the models due to the missing TMD, and the ligand bTSH were removed. In the initial placement of the two partners the ECD was placed arbitrarily in an upright position above the interface with the TMD. The initial perturbation included a random spin between 0 and 360º around and a random tilt between 0 and 90º along the sliding axis (roughly parallel to the membrane normal). For this purpose, the tilt option was implemented and incorporated into the Rosetta Software suite, allowing a random tilt within a predefined limit during the initial perturbation step of the docking protocol (28). During docking a cross interface disulfide between C284 and C408 was enforced. Furthermore, the low-resolution step of the docking protocol was repeated until the Cβ-distance between C284 and C408 was below 15 Å. For each ECD/TMD combination 1000 models were built. The S281/I486 Cβ-distance for each model was determined with Rosetta's contactMap protocol and the interface energies with the InterfaceAnalyzerMover (29). For remodeling of the linker region (K401-I411) two sets were selected: i) all models of the best 100 by dG separated with a S281-I486 Cβ-distance below 15 Å (57 models) and ii) all models with dG separated below -6 and a S281-I486 Cβ-distance below 10 Å (41 models). For each of these, 25 loopmodels were generated with a subsequent relaxation step. The resulting models were again clustered with Calibur. The best scoring models of the 10 largest clusters have been deposited at the model archive (http://dx.doi.org/10.5452/ma-aptif). Contact maps were generated for each cluster as well as for all models with a Cβ-distance cutoff of 8 Å. For the best scoring structure of each cluster the position of the hormone and the position and environment of the sulfated tyrosine residue recapitulated those of the initial homology model of the extracellular domain. The junctions were remodeled (25 decoys), followed by relaxation of the entire structure.

Visualization and image generation was done using the PyMOL Molecular Graphics System (Version 1.5.0.4 Schrödinger, LLC).

RESULTS AND DISCUSSION

Strategy for TSHR structure prediction based on chemical crosslinking and mutation data

Structural modelling of the full-length TSHR was based on structural templates resolved by x-ray crystallography of the GPHR-ECD (11, 25) as well as the TMD of class A GPCRs (Fig. 2). Experimental data from chemical crosslinking of the soluble TSHR-ECD with bovine TSH (bTSH) was incorporated to guide and evaluate the homology modelling of the TSHR-ECD/TSH complex. A number of class A GPCR experimental structures were incorporated into homology modelling of the TSHR-TMD by utilizing the multiple template approach of RosettaCM (27). The models of the ECD and the TMD were combined by docking with subsequent remodelling of the linker region. In this step structural flexibility of the interfaces was incorporated by combining various homology models of the ECD and TMD during docking. The putative contact of the ECD residue S281 with the TMD was identified and verified by double mutant cycle analysis. This contact was used to guide and evaluate placement of the ECD in relation to the TMD during docking, along with the cross-interface disulfide (11, 30). To gain information on frequently occurring ECD/TMD orientations and specific interface contacts, the final ensemble of models was analyzed by clustering and contact maps. Plausibility of the most frequent ECD/TMD orientations was verified by reintroduction of the ligand into the models.

Downloaded from http://www.jbc.org/ at Vanderbilt University - Biomedical & Science/Engineering Libraries on November 7, 2016

Mass spectrometry analysis confirms glycosylation, sulfation, and proteolytic cleavage of the extracellular domain

Glycosylation - Mass spectrometric analysis of the soluble TSHR-ECD after tryptic digestion identified fragments covering 80% of the protein sequence of the utilized construct. The analysis of glycosylation sites revealed complete glycosylation of three out of six putative sites within the ECD, at Asn77/113/177, and a partial glycosylation of Asn302 (31). Due to the absence of detected proteolytic peptides covering the remaining two sites (Asn99/198), glycosylation of these sites could not be determined by MS.

Sulfation - Sulfation of the TSHR-ECD was identified at position Y385, as suggested by Costagliola *et al*. (10), as well as at position Y387. Sulfation was typically identified at a single site or at both sites simultaneously; the peptide representing the non-sulfated form of TSHR was rarely observed. However, the mutagenesis data clearly show that the functional importance of tyrosine sulfation is exclusively attributed to Y385, with no functional compensation by Y387. However, whereas sulfation of Y385 and Y387 was determined in a truncated ECD, functional data was gathered from the full-length receptor. Given that secondary structure supposedly has a major influence on sulfation (32), and with the structural influence of the TMD on the HR (17), there might be a discrepancy between sulfation of the truncated and the full-length TSHR, with sulfation of Y387 occurring only in the truncated receptor.

Proteolytic cleavage - Wadsworth *et al*. suggested that residues A317-F366 are posttranslationally removed with no apparent effect on TSHR function (33). Analysis of proteolytic cleavage of the TSHR by MS confirmed C-terminal cleavage between position F366 and G367 by detection of a proteolytic peptide (G367-K371). Yet no peptide confirming the N-terminal cleavage site between N316 and A317 was detected. Recent studies suggest that excision occurs by successive removal of small fragments resulting in ragged boundaries (34-36).

Homology models of the TSHR-ECD/TSH complex consistent with chemical crosslinking data

The TSHR-ECD/TSH complex was studied by chemical crosslinking and MS using four different amino-reactive crosslinking reagents with differing spacer lengths. Prior to crosslinking the tight binding of bovine TSH to the TSHR-ECD was verified by surface plasmon resonance (SPR) spectroscopy. Steady-state analysis indicates a two-site binding model as previously reported (13). Seventeen unique distance restraints could be determined within the TSHR-ECD/TSH complex (Fig. 1 and Table 1). These included nine receptor-hormone crosslinks, two crosslinks between the subunits of the hormone, and three within the receptor and the α-chain of the hormone, respectively. A comparative model of the TSHR-ECD/TSH complex was constructed using the experimentally determined structure of the FSHR-ECD/FSH complex (PDB 4ay9 (11)) as template. The N-terminal residues for this model up to L57 (L51 FSHR) were taken from the TSHR-LRR domain structure (PDB 2xwt (25)). The majority of the XL-MS restraints are consistent with this comparative model (Fig. 1B). Specifically, of the 1800 models in the ensemble (top 90% by score), 99% fulfil 12 or more of the 17 crosslinks. Two crosslinks are violated in all models (Fig. 1 - ID 3 and 4), an effect that we attribute to a conformational change induced by the crosslinker (read below). If a protein exists in multiple conformations, it is sufficient if one conformation has the amino acids in close proximity to observe the crosslink. In turn, not all conformations need to fulfil all cross-links simultaneously in flexible regions of the protein. Crosslinks ID 5, 8, and 9 connect flexible regions which are assumed to be present in multiple conformations. Accordingly, we expect these to be violated in a higher fraction of the models. Crosslinks within the hormone (ID 6, 7, 10) or the receptor (ID 1, 11, 15) confirm the general fold of the hormone and the ECD (Fig. 3A). Crosslinks between the hormone and receptor close to loop 1 and 3 (α-L1/3) of the hormone's α-subunit (ID 8, 13) as well as to α-L2 at the opposite side of the hormone (ID 2, 12, 16) confirm a similar binding mode of bTSH as reported for the FSHR-ECD/FSH experimental structure (11, 37) (Fig. 3B).

Structural plasticity in the curvature of the LRR domain

Interestingly, two crosslinks (Fig. 1 - ID 2 and 17) exceeded the expected maximal Cβ-distance of the crosslinking reagent, based on an initial model of the TSHR-ECD/TSH complex from the structure

Downloaded from http://www.jbc.org/ at Vanderbilt University - Biomedical & Science/Engineering Libraries on November 7, 2016

of the TSHR-LRR domain (PDB 2xwt (25)) up to S234 (S226 FSHR) and the HR of the FSHR-ECD/FSH structure. Superimposition of the two employed templates revealed a reduced curvature of the TSHR-LRR domain at the transition region of the templates, which results in an increased distance between the hormone and the N-terminal section of the receptor (Fig. 3F). These models also display less favourable Cβ-distances for three other crosslinks (ID: 3, 12 and14). A steeper curvature is also observed in the structure of the FSHR-LRR domain (PDB 1xwd (37)). Therefore the differences in curvature are most likely sequence specific (38) and not due the inclusion of the HR.

Conformation of the TSHR-HR

Crosslinks between the receptors HR and the TSH hormone (ID 8, 9 and 13) confirm a significant interface between the HR with the hormone that could be important for signal transduction (Fig. 1C). It has previously been suggested that a part of the HR, including the region which is subjected to proteolytic cleavage within the TSHR, is intrinsically disordered (39). This hypothesis is supported by the FSHR-ECD crystal structure (PDB 4ay9 (11)), where no density is observed for the respective region.

A TSHR-ECD/TSH specific interaction between TSHR E34 and TSH β-chain K101

Visual inspection of the best scoring models also suggests a potential TSHR specific interaction at the N-terminal end of the LRR domain due to spatial proximity of the sidechains of E34 of the TSHR with K101 of the TSH β-chain observed in two models (Fig. 3E). Interestingly a TSHR mutation of E34 (E34K) has been detected in patients with hypothyroidism (40). However, with no detailed binding data and only a slight impairment of Gs signaling reported, the putative contribution of an E34/K101 interaction to binding affinity and specificity is most likely only marginal.

Spatial proximity between the TSH α-chain N-terminus and TSH β-chain K101

Next to this interaction with the receptor a crosslink between K101 and the N-terminus of the α-chain was detected (ID 5) implying a close proximity of both termini (Fig. 3C). Yet the residues are within the expected distance in only 2% of the models. Because the N-terminal amino acids of the α-chain are not ordered in any of the crystallographic structures of the human GPHs (11, 37, 41-44), this region is expected to be flexible. The bovine GPH α-chain features four additional amino acids, possibly increasing flexibility in the region (45).

Crosslinks ID 3 and 4 are violated in all comparative models

DST yielded two further crosslinks to the α-L2 (ID 3 and 4), which are incompatible with all models (Fig. 3D). In contrast to crosslink 5, the connected residues are in structurally well-defined regions. However, conformational changes in α-L2, including a disintegration of the helical fragment potentially induced by the coupling of DST, could be sufficient for the crosslink to be established. Alternatively, binding of the hormone to a second, low-affinity binding site as suggested previously (13, 46, 47) could also be associated with a closer proximity of the crosslinked residues. A third explanation for the controversial crosslinks is the possibility that the crosslink is not established between the hormone and the ECD it is bound to, but rather with the ECD of the adjacent ECD/hormone complex in the putative trimer structure (48). However, analysis of this scenario reveals that the Cβ-distance to the HR within the ECD/hormone complex does not differ much from the distance to the HR in the adjacent complex. Yet, sidechain orientation and surface distance are more favorable for a crosslink to the HR of the adjacent ECD/hormone complex (Fig. 3G).

Identification and verification of an ECD/ECL1 contact between S281 and I486 by double mutant cycle analysis

It has been demonstrated that distant mutations result in synergistic receptor activation (49) and mutations in close proximity in a more complex pattern dependent on the sidechain substitutions (20). Several constitutively activating mutations (CAMs) of S281 (FSHR S273, LHR S277) in the C-terminal helix of the ECD (50-52) mark this residue as an important component of the interface with the TMD (50, 53). To confirm specific contacts of the putative ECD/TMD interface we have combined the CAM S281I with two TMD CAMs of the comparably long ECL1 (I486S, T490A) and ECL2 (I568T). For mutations of I486 and I568, constitutive activity has only been

Downloaded from http://www.jbc.org/ at Vanderbilt University - Biomedical & Science/Engineering Libraries on November 7, 2016

observed in presence of the ECD (54). Combination of S281I with I486S (LRA 22) yields a receptor with similar constitutive activity to the I486S single mutant (LRA 19) (Table 2). The absence of an additive effect suggests a shared leverage point of constitutive receptor activation and close spatial proximity. Targeted mutation of both residues to cysteines resulted in a receptor devoid of hormone-induced activation of the Gs and Gq signaling pathway (Fig. 4 and Table 2). Even though the ligand-binding properties and cell surface expression of the double mutant are within the range of the single mutants, only the latter show ligand-induced receptor activation. Based on these observations the missing change in activity of the double mutant upon ligand binding is putatively caused by the presence of a disulfide bond between the introduced cysteines. The presence of a disulfide bond in this region critical to receptor activation most likely locks the receptor in a partially activated conformation and thus prevents signal propagation. In order for this bond to form, the two residues therefore have to be in close structural proximity in the receptor. Exchange of both residues to aspartate yields a receptor with retained ligand binding but no ligand-induced activation of G-protein signaling. This observation is consistent with the notion that repulsive forces between the negatively charged aspartate side chains prevent signal propagation. Conformational changes at the ECD/ECL1 interface, including a relative repositioning of S281 and I486, are therefore a requirement for receptor activation (Table 2).

T490 and I568 are not in direct contact with S281

With the confirmation of the S281/ECL1 contact, we tested whether S281 is proximal to T490 in ECL1 and I568 in ECL2 (49). However, even though combining the two cysteine mutations has a detrimental effect on cell surface expression and ligand-induced Gq-signalling, no loss of Gs-activation was observed (Table 2). Therefore, T490 is most likely not in close proximity to S281. Combination of the constitutively activating mutations (CAMs) S281I (LRA 37) and I568T (LRA 30) is synergistic yielding a receptor with increased constitutive activity (LRA 78) and high levels of basal cAMP production at 92% of the activated *wt* receptor level, despite a cell surface expression of only 27% compared to the *wt*. We conclude that S281I and I568T are unlikely to be in direct contact. Notably, combination of the CAM S281I and I568T is associated with no apparent ligand-induced receptor activation despite retained binding affinity. This suggests that the S281I/I568T double mutant adopts the conformation of the fully activated receptor lacking ligand-induced activation. A similar phenotype has been previously associated with full receptor activation (49). In that study mutations in all three extracellular loops were necessary, whereas in our case substitutions at the ECD/ECL1 and ECL2/TM6 (55) interface were sufficient to enforce the activated conformation.

Docking of ECD and TMD to generate a full-length receptor model

Whereas homology models of the ECD showed little structural variations in the presumed interface to the TMD surrounding S281, models of the TMD showed greater flexibility especially in ECL1 (Fig. 5), which is, with 8-10 additional amino acids, significantly longer than in most class A GPCRs. Accordingly, the five best-scoring, representative ECD models were docked with the 30 best-scoring, representative models of the TMD. Best-scoring, representative models were chosen by clustering to mimic a conformational selection process. Cluster centers for the TMD included models derived both from TMD templates in an ‘active’ conformation and from those in an ‘inactive’ conformation. Analysis of the interaction energy of docked models compared with the S281/I486 Cβ-distance reveals an energy funnel at a distance of 12.5 Å (Fig. 6A) with a very similar orientation of the ECD towards the TMD (Fig. 6C) in an upright position with S281 facing towards ECL1 (Fig. 7). The best scoring models with an S281/I486 Cβ-distance below 10 Å show greater diversity in the relative orientation of ECD and TMD (Fig. 6B). With a comparatively large S281/I486 Cβ-distance, the cluster at 17.5 Å (Fig 6A) was not considered for further analysis. Addition of the hormone to the full receptor models does not result in an overlap of the hormone with the membrane in any of the structures, and thus confirms the plausibility of the observed ECD orientations. To allow a free exploration of ECD/TMD orientations, the flexible linker region between ECD and TMD was constructed after completion of the docking simulation. The superior energy of the model is preserved when compared to

Downloaded from http://www.jbc.org/ at Vanderbilt University - Biomedical & Science/Engineering Libraries on November 7, 2016

models with a S281/I486 Cβ-distance below 10 Å (Fig. 8A). Strikingly, in the final model I486 is part of an extended transmembrane helix 3 with the sidechain facing away from the interface with the ECD (Fig. 7). In contrast the models with a shorter S281/I486 Cβ-distance lack an extended TM3, enabling a loop conformation with the I486 sidechain facing towards the ECD. These models also show a small helical segment within ECL1 similar to the smoothened receptor ((56); PDB 4o9r) and a conformation of the C-terminal part similar to the WXFG motif present in most class A GPCR structures (WQTG in all three GPHRs), to which a pivotal role in ligand mediated receptor activation is attributed (57) (Fig. 8B). Mutations of W488 in the TSHR result in a drastically reduced cell surface expression, suggesting a similar importance (49). The comparison of contact maps of the largest and best scoring cluster to the largest cluster with an average S281/I486 distance below 10 Å shows that the first cluster is consistent with placing Y279 and Y481 in the environment of S281 as has been suggested previously (50), whereas the latter displays the experimentally determined close proximity of S281 and I486 (Fig. 8C).

Multiple conformations involved in TSHR activation

It is possible that the two observed ECL1 conformations represent different stages during GPCR activation. The extended, low energy TM3 conformation is similar to the activated state. The loop conformation observed in the fourth cluster would represent the basal state of the receptor. In this scenario T490 is part of the small fragment that changes its conformation between the fold of the WXFG motif and an extended TM3 during activation (Fig. 7 and Fig. 8B). This is supported by the observation that substitution at this position to alanine, which has a higher helix probability than threonine (58), can facilitate the transition towards the activated conformation as observed in the CAM T490A. The high conservation of the region surrounding S281 and ECL1 within GPHRs as well as the shared propensity for constitutive receptor activation by mutations of S281 suggests an identical mechanism of activation and a shared ECD/ECL1 interface within GPHRs. The presented modeling approach can therefore be easily extended to the remaining two GPHRs. The final ensemble of models offers important insights into the likely mechanism of GPHR activation. By incorporating experimental data from chemical crosslinking coupled with MS fragment analysis and targeted receptor mutation, the quality and relevance of the final models set was significantly increased and enabled the generation of the first experimentally supported full-length models of a GPHR.

ACKNOWLEDGEMENTS

We thank S. Costagliola (Université libre de Bruxelles) for providing the GPI-anchored TSHR-ECD as well as PI-PLC. We also thank C. Schaarschmidt and S. Fiedler for their excellent technical assistance. This work was supported by a grant from the Deutsche Forschungsgemeinschaft (DFG, Ja 1927/1-2), ESF Investigator group GPCR 2, and a grant from the Else Kröner-Fresenius-Stiftung (2012_A244).

CONFLICT OF INTEREST:

The authors declare that they have no conflicts of interest with the contents of this article.

AUTHOR CONTRIBUTIONS:

JS, SH, HJ, MvB, SK, JM and RP conceived the study and designed research. JS performed site-directed mutagenesis and functional characterization of the receptor. JS and MBMN expressed, purified and crosslinked the soluble extracellular domain. MBMN and SK performed the mass spectrometric measurements and analysis. MBMN and VH performed the SPR experiment. JS and RM performed the molecular modelling. JS, MBMN, SK, JM, and RP wrote the paper. All authors analyzed data and approved the final version of the manuscript.

REFERENCES

1. Pierce, J. G., and Parsons, T. F. (1981) Glycoprotein Hormones: Structure and Function. *Annu. Rev. Biochem.* **50**, 465–495

Downloaded from http://www.jbc.org/ at Vanderbilt University - Biomedical & Science/Engineering Libraries on November 7, 2016

2. Braun, T., Schofield, P. R., and Sprengel, R. (1991) Amino-terminal leucine-rich repeats in gonadotropin receptors determine hormone selectivity. *EMBO J*. **10**, 1885–1890
3. Jiang, X., Dreano, M., Buckler, D. R., Cheng, S., Ythier, A., Wu, H., Hendrickson, W. A., and Tayar, N. E. (1995) Structural predictions for the ligand-binding region of glycoprotein hormone receptors and the nature of hormone–receptor interactions. *Structure*. **3**, 1341–1353
4. Kleinau, G., and Krause, G. (2009) Thyrotropin and Homologous Glycoprotein Hormone Receptors: Structural and Functional Aspects of Extracellular Signaling Mechanisms. *Endocr Rev*. **30**, 133–151
5. Heitman, L. H., Kleinau, G., Brussee, J., Krause, G., and IJzerman, A. P. (2012) Determination of different putative allosteric binding pockets at the lutropin receptor by using diverse drug-like low molecular weight ligands. *Mol. Cell. Endocrinol.* **351**, 326–336
6. Jäschke, H., Neumann, S., Moore, S., Thomas, C. J., Colson, A. O., Costanzi, S., Kleinau, G., Jiang, J. K., Paschke, R., Raaka, B. M., Krause, G., and Gershengorn, M. C. (2006) A Low Molecular Weight Agonist Signals by Binding to the Transmembrane Domain of Thyroid-stimulating Hormone Receptor (TSHR) and Luteinizing Hormone/Chorionic Gonadotropin Receptor (LHCGR). *J Biol Chem*. **281**, 9841–9844
7. Neumann, S., Pope, A., Geras-Raaka, E., Raaka, B. M., Bahn, R. S., and Gershengorn, M. C. (2012) A Drug-Like Antagonist Inhibits Thyrotropin Receptor–Mediated Stimulation of cAMP Production in Graves' Orbital Fibroblasts. *Thyroid*. **22**, 839–843
8. Kursawe, R., and Paschke, R. (2007) Modulation of TSHR signaling by posttranslational modifications. *Trends Endocrinol. Metab.* **18**, 199–207
9. Chazenbalk, G. D., Tanaka, K., McLachlan, S. M., and Rapoport, B. (1999) On the Functional Importance of Thyrotropin Receptor Intramolecular Cleavage 1. *Endocrinology*. **140**, 4516–4520
10. Costagliola, S., Panneels, V., and Bonomi, M. (2002) Tyrosine sulfation is required for agonist recognition by glycoprotein hormone receptors. *EMBO J*. **21**, 504–513
11. Jiang, X., Liu, H., Chen, X., Chen, P. H., Fischer, D., Sriraman, V., Yu, H. N., Arkinstall, S., and He, X. (2012) Structure of follicle-stimulating hormone in complex with the entire ectodomain of its receptor. *Proc Natl Acad Sci USA*. **109**, 12491–12496
12. Kalkhof, S., and Sinz, A. (2008) Chances and pitfalls of chemical cross-linking with amine-reactive N-hydroxysuccinimide esters. *Anal. Bioanal. Chem.* **392**, 305–312
13. Cornelis, S., Uttenweiler-Joseph, S., Panneels, V., Vassart, G., and Costagliola, S. (2001) Purification and Characterization of a Soluble Bioactive Amino-Terminal Extracellular Domain of the Human Thyrotropin Receptor. *Biochemistry*. **40**, 9860–9869
14. Carter, P. J., Winter, G., Wilkinson, A. J., and Fersht, A. R. (1984) The use of double mutants to detect structural changes in the active site of the tyrosyl-tRNA synthetase (Bacillus stearothermophilus). *Cell*. **38**, 835–840
15. Horovitz, A. (1996) Double-mutant cycles: a powerful tool for analyzing protein structure and function. *Folding and Design*. **1**, R121–R126
16. Leaver-Fay, A., Tyka, M., Lewis, S. M., Lange, O. F., Thompson, J., Jacak, R., Kaufman, K. W., Renfrew, P. D., Smith, C. A., Sheffler, W., Davis, I. W., Cooper, S., Treuille, A., Mandell, D. J., Richter, F., Ban, Y.-E. A., Fleishman, S. J., Corn, J. E., Kim, D. E., Lyskov, S., Berrondo, M., Mentzer, S., Popović, Z., Havranek, J. J., Karanicolas, J., Das, R., Meiler, J., Kortemme, T., Gray, J. J., Kuhlman, B., Baker, D., and Bradley, P. (2011) Rosetta3: An Object-Oriented Software Suite for the Simulation and Design of Macromolecules. in *Biopolymers* (Kalia, S., and Avérous, L. eds), pp. 545–574, Methods in Enzymology, Elsevier, **487**, 545–574
17. Schaarschmidt, J., Huth, S., Meier, R., Paschke, R., and Jaeschke, H. (2014) Influence of the Hinge Region and Its Adjacent Domains on Binding and Signaling Patterns of the Thyrotropin and Follitropin Receptor. *PLoS ONE*. **9**, e111570
18. Jaeschke, H., Schaarschmidt, J., Günther, R., and Mueller, S. (2011) The Hinge Region of the TSH Receptor Stabilizes Ligand Binding and Determines Different Signaling Profiles of Human and Bovine TSH. *Endocrinology*. **152**, 3986–3996

Downloaded from http://www.jbc.org/ at Vanderbilt University - Biomedical & Science/Engineering Libraries on November 7, 2016

19. Mueller, S., Kleinau, G., Jaeschke, H., Paschke, R., and Krause, G. (2008) Extended hormone binding site of the human thyroid stimulating hormone receptor: distinctive acidic residues in the hinge region are involved in bovine thyroid stimulating hormone binding and receptor activation. *J Biol Chem*. **283**, 18048–18055
20. Jaeschke, H., Schaarschmidt, J., Eszlinger, M., Huth, S., Puttinger, R., Rittinger, O., Meiler, J., and Paschke, R. (2014) A Newly Discovered TSHR Variant (L665F) Associated With Nonautoimmune Hyperthyroidism in an Austrian Family Induces Constitutive TSHR Activation by Steric Repulsion Between TM1 and TM7. *J. Clin. Endocrinol. Metab.* **99**, E2051–E2059
21. Hampf, M., and Gossen, M. (2006) A protocol for combined Photinus and Renilla luciferase quantification compatible with protein assays. *Anal. Biochem.* **356**, 94–99
22. Müller, S. A., Pernitzsch, S. R., Haange, S.-B., Uetz, P., Bergen, von, M., Sharma, C. M., and Kalkhof, S. (2015) Stable isotope labeling by amino acids in cell culture based proteomics reveals differences in protein abundances between spiral and coccoid forms of the gastric pathogen Helicobacter pylori. *J. Proteomics*. **126**, 34–45
23. Götze, M., Pettelkau, J., Schaks, S., Bosse, K., Ihling, C. H., Krauth, F., Fritzsche, R., Kühn, U., and Sinz, A. (2011) StavroX—A Software for Analyzing Crosslinked Products in Protein Interaction Studies. *J. Am. Soc. Mass Spectrom.* **23**, 76–87
24. Raman, S., Vernon, R., Thompson, J., Tyka, M., Sadreyev, R., Pei, J., Kim, D., Kellogg, E., DiMaio, F., Lange, O., Kinch, L., Sheffler, W., Kim, B.-H., Das, R., Grishin, N. V., and Baker, D. (2009) Structure prediction for CASP8 with all-atom refinement using Rosetta. *Proteins*. **77**, 89–99
25. Sanders, P., Young, S., Sanders, J., Kabelis, K., Baker, S., Sullivan, A., Evans, M., Clark, J., Wilmot, J., Hu, X., Roberts, E., Powell, M., Núñez Miguel, R., Furmaniak, J., and Rees Smith, B. (2011) Crystal structure of the TSH receptor (TSHR) bound to a blocking-type TSHR autoantibody. *J Mol Endocrinol*. **46**, 81–99
26. Li, S. C., and Ng, Y. K. (2010) Calibur: a tool for clustering large numbers of protein decoys. *BMC Bioinform.* **11**, 25
27. Song, Y., DiMaio, F., Wang, R. Y.-R., Kim, D., Miles, C., Brunette, T. J., Thompson, J., and Baker, D. (2013) High-Resolution Comparative Modeling with RosettaCM. *Structure*. **21**, 1735–1742
28. Chaudhury, S., Berrondo, M., Weitzner, B. D., Muthu, P., Bergman, H., and Gray, J. J. (2011) Benchmarking and analysis of protein docking performance in Rosetta v3.2. *PLoS ONE*. **6**, e22477
29. Stranges, P. B., and Kuhlman, B. (2013) A comparison of successful and failed protein interface designs highlights the challenges of designing buried hydrogen bonds. *Protein Sci.* **22**, 74–82
30. Ho, S.-C., Goh, S.-S., Li, S., Khoo, D. H.-C., and Paterson, M. (2008) Effects of Mutations Involving Cysteine Residues Distal to the S281HCC Motif at the C-Terminus on the Functional Characteristics of a Truncated Ectodomain-Only Thyrotropin Receptor Anchored on Glycosylphosphatidyl-Inositol. *Thyroid*. **18**, 1313–1319
31. Nagayama, Y., Nishihara, E., Namba, H., Yamashita, S., and Niwa, M. (2000) Identification of the sites of asparagine-linked glycosylation on the human thyrotropin receptor and studies on their role in receptor function and expression. *J. Pharmacol. Exp. Ther.* **295**, 404–409
32. Nicholas, H. B., Chan, S. S., and Rosenquist, G. L. (1999) Reevaluation of the Determinants of Tyrosine Sulfation. *Endocrine*. **11**, 285–292
33. Wadsworth, H., Chazenbalk, G., Nagayama, Y., Russo, D., and Rapoport, B. (1990) An insertion in the human thyrotropin receptor critical for high affinity hormone binding. *Science*. **249**, 1423–1425
34. Graves, P., Pritsker, A., and Davies, T. F. (1999) Post-Translational Processing of the Natural Human Thyrotropin Receptor: Demonstration of More than Two Cleavage Sites 1. *J. Clin. Endocrinol. Metab.* **84**, 2177–2181
35. Tanaka, K., Chazenbalk, G. D., McLachlan, S. M., and Rapoport, B. (2000) Evidence that Cleavage of the Thyrotropin Receptor Involves a“ Molecular Ruler” Mechanism: Deletion of

Downloaded from http://www.jbc.org/ at Vanderbilt University - Biomedical & Science/Engineering Libraries on November 7, 2016

Amino Acid Residues 305–320 Causes a Spatial Shift in Cleavage Site 1 Independent of Amino Acid Motif 1. *Endocrinology*. **141**, 3573–3577
36. Hamidi, S., Chen, C.-R., Mizutori-Sasai, Y., McLachlan, S. M., and Rapoport, B. (2011) Relationship between Thyrotropin Receptor Hinge Region Proteolytic Posttranslational Modification and Receptor Physiological Function. *Mol. Endocrinol.* **25**, 184–194
37. Fan, Q. R., and Hendrickson, W. A. (2005) Structure of human follicle-stimulating hormone in complex with its receptor. *Nature*. **433**, 269–277
38. Jiang, X., Dias, J. A., and He, X. (2014) Structural biology of glycoprotein hormones and their receptors: Insights to signaling. *Mol. Cell. Endocrinol.* **382**, 424–451
39. Mueller, S., Jaeschke, H., Günther, R., and Paschke, R. (2010) The hinge region: an important receptor component for GPHR function. *Trends Endocrinol. Metab.* **21**, 111–122
40. De Marco, G., Agretti, P., Camilot, M., Teofoli, F., Tatò, L., Vitti, P., Pinchera, A., and Tonacchera, M. (2009) Functional studies of new TSH receptor (TSHr) mutations identified in patients affected by hypothyroidism or isolated hyperthyrotrophinaemia. *Clin. Endocrinol.* **70**, 335–338
41. Fox, K. M., Dias, J. A., and Van Roey, P. (2001) Three-Dimensional Structure of Human Follicle-Stimulating Hormone. *Mol. Endocrinol.* **15**, 378–389
42. Wu, H., Lustbader, J. W., Liu, Y., Canfield, R. E., and Hendrickson, W. A. (1994) Structure of human chorionic gonadotropin at 2.6 å resolution from MAD analysis of the selenomethionyl protein. *Structure*. **2**, 545–558
43. Lapthorn, A. J., Harris, D. C., Littlejohn, A., Lustbader, J. W., Canfield, R. E., Machin, K. J., Morgan, F. J., and Isaacs, N. W. (1994) Crystal structure of human chorionic gonadotropin. *Nature*. **369**, 455–461
44. Tegoni, M., Spinelli, S., Verhoeyen, M., Davis, P., and Cambillau, C. (1999) Crystal structure of a ternary complex between human chorionic gonadotropin (hCG) and two Fv fragments specific for the α and β-subunits. *J Mol Biol*. **289**, 1375–1385
45. Mueller, S., Kleinau, G., Szkudlinski, M. W., Jaeschke, H., Krause, G., and Paschke, R. (2009) The Superagonistic Activity of Bovine Thyroid-stimulating Hormone (TSH) and the Human TR1401 TSH Analog Is Determined by Specific Amino Acids in the Hinge Region of the Human TSH Receptor. *J Biol Chem*. **284**, 16317–16324
46. Urizar, E., Montanelli, L., Loy, T., Bonomi, M., Swillens, S., Gales, C., Bouvier, M., Smits, G., Vassart, G., and Costagliola, S. (2005) Glycoprotein hormone receptors: link between receptor homodimerization and negative cooperativity. *EMBO J*. **24**, 1954–1964
47. Zoenen, M., Urizar, E., Swillens, S., Vassart, G., and Costagliola, S. (2012) Evidence for activity-regulated hormone-binding cooperativity across glycoprotein hormone receptor homomers. *Nat Commun*. **3**, 1007
48. Jiang, X., Fischer, D., Chen, X., Mckenna, S. D., Liu, H., Sriraman, V., Yu, H. N., Goutopoulos, A., Arkinstall, S., and He, X. (2014) Evidence for Follicle-stimulating Hormone Receptor as a Functional Trimer. *J Biol Chem*. **289**, 14273–14282
49. Kleinau, G., Jaeschke, H., Mueller, S., Raaka, B. M., Neumann, S., Paschke, R., and Krause, G. (2008) Evidence for cooperative signal triggering at the extracellular loops of the TSH receptor. *FASEB J.* **22**, 2798–2808
50. Jaeschke, H., Neumann, S., Kleinau, G., Mueller, S., Claus, M., Krause, G., and Paschke, R. (2006) An Aromatic Environment in the Vicinity of Serine 281 Is a Structural Requirement for Thyrotropin Receptor Function. *Endocrinology*. **147**, 1753–1760
51. Nakabayashi, K., Kudo, M., Hsueh, A. J. W., and Maruo, T. (2003) Activation of the luteinizing hormone receptor in the extracellular domain. *Mol. Cell. Endocrinol.* **202**, 139–144
52. Montanelli, L., Van Durme, J. J. J., Smits, G., Bonomi, M., Rodien, P., Devor, E. J., Moffat-Wilson, K., Pardo, L., Vassart, G., and Costagliola, S. (2004) Modulation of Ligand Selectivity Associated with Activation of the Transmembrane Region of the Human Follitropin Receptor. *Mol. Endocrinol.* **18**, 2061–2073

Downloaded from http://www.jbc.org/ at Vanderbilt University - Biomedical & Science/Engineering Libraries on November 7, 2016

53. Kleinau, G., Neumann, S., Grüters, A., Krude, H., and Biebermann, H. (2013) Novel insights on thyroid-stimulating hormone receptor signal transduction. *Endocr Rev*. **34**, 691–724
54. Vlaeminck-Guillem, V., Ho, S.-C., Rodien, P., Vassart, G., and Costagliola, S. (2002) Activation of the cAMP Pathway by the TSH Receptor Involves Switching of the Ectodomain from a Tethered Inverse Agonist to an Agonist. *Mol. Endocrinol.* **16**, 736–746
55. Kleinau, G., Claus, M., Jaeschke, H., Mueller, S., Neumann, S., Paschke, R., and Krause, G. (2006) Contacts between Extracellular Loop Two and Transmembrane Helix Six Determine Basal Activity of the Thyroid-stimulating Hormone Receptor. *J Biol Chem*. **282**, 518–525
56. Weierstall, U., James, D., Wang, C., White, T. A., Wang, D., Liu, W., Spence, J. C. H., Bruce Doak, R., Nelson, G., Fromme, P., Fromme, R., Grotjohann, I., Kupitz, C., Zatsepin, N. A., Liu, H., Basu, S., Wacker, D., Han, G. W., Katritch, V., Boutet, S., Messerschmidt, M., Williams, G. J., Koglin, J. E., Marvin Seibert, M., Klinker, M., Gati, C., Shoeman, R. L., Barty, A., Chapman, H. N., Kirian, R. A., Beyerlein, K. R., Stevens, R. C., Li, D., Shah, S. T. A., Howe, N., Caffrey, M., and Cherezov, V. (2014) Lipidic cubic phase injector facilitates membrane protein serial femtosecond crystallography. *Nat Commun*. **5**, 3309
57. Klco, J. M., Nikiforovich, G. V., and Baranski, T. J. (2006) Genetic Analysis of the First and Third Extracellular Loops of the C5a Receptor Reveals an Essential WXFG Motif in the First Loop. *J Biol Chem*. **281**, 12010–12019
58. Meiler, J., Mueller, M., Zeidler, A., and Schmaeschke, F. (2001) Generation and evaluation of dimension-reduced amino acid parameter representations by artificial neural networks. *J. Mol. Model.* **7**, 360–369

Downloaded from http://www.jbc.org/ at Vanderbilt University - Biomedical & Science/Engineering Libraries on November 7, 2016

TABLE LEGENDS

TABLE 1. Crosslinked peptides of the TSHR-ECD/TSH complex identified by mass spectrometry and resulting estimated cutoff distances for structural modelling

TABLE 2. Functional characterization of the wt and mutant TSHR. COS-7 (HEK_{GT} for NFAT) cells were transiently transfected with the respective DNA constructs. Values are normalized to wt level (basal state where applicable). Data are presented as mean values and standard error of at least three independent experiments, each carried out in duplicates. The pcDNA3.1/Zeo vector was used as a control.

FIGURE LEGENDS

FIGURE 1. Schematic representation and identified crosslinks of the TSHR/TSH complex. A Schematic representation of the TSHR/TSH complex including disulfides, crosslinked residues identified by mass spectrometry and significant residues of the TSHR, including residues with reported constitutively activating mutations (S281, I486, I568), the sulfation site (Y385) and boundaries of the model within the HR (F381, S304). The respective spacer-length of the crosslinking reagents is specified in the figure legend. **B** Boxplot of Cβ-distance distance distribution between residues connected by chemical crosslinking within the homology models of the TSHR-ECD/TSH complex. The employed crosslink-specific cutoff distance (Table 1) is indicated by a dashed line in grey. Crosslinks 8 and 9 include one residue located in the part of the HR not included within the models. For these, the distance to the closest residue included in the models is reported and the missing residues are considered in the cutoff distance. **C** Crosslinks (green lines) between the hinge region of the TSHR (blue) and the hormone (α-chain – red, β-chain - yellow) suggest that the HR, including the part not resolved in the FSHR-ECD/FSH template and therefore not included in the homology models, is oriented towards the hormone and most likely also contributes to ligand binding.

FIGURE 2. Strategy for generating full-length GPHR models. An integrated structural biology approach combining computational techniques (**A-D**) with experimental data (**E1-2**). Homology models were constructed using Rosetta 3 for the TSHR-ECD (**A1-2**) and the multi-template approach of RosettaCM for the TSHR-TMD (**B1**). Chemical crosslinking of the soluble TSHR-ECD yielded 17 crosslinks that were used to guide template selection and evaluate the models of the TSHR-ECD (**E1**). The model sets were further analyzed by clustering analysis using Calibur (**A3** and **B2**). Models were selected based on energy and cluster size. The combination of 30 TSHR-TMD models with 5 TSHR-ECD models by docking yielded 150 000 docked models (**C1**). During docking a cross interface disulfide between C284 and C408 was enforced. From the docked poses ~100 models were selected based on interface score and agreement with the experimentally verified contact of S281 with I486 (E2) for reconstruction of the linker region (K401-I411, **C2**). The model set of the full length TSHR was further analyzed by contact maps (**D1**) and clustering (**D2**). Feasibility of the full-length models was verified by reintroduction of the ligand and remodelling of the "thumb"-region (**D2**).

FIGURE 3. Homology models of the TSHR-ECD(blue)/TSH(α-chain – red, β-chain – yellow) complex. Crosslinks (green dotted lines) confirm the fold (**A**) of the domains and (**B**) a similar binding mode of TSH as observed for FSH to the FSHR-ECD. **C** The crosslink (green line) between the N-terminus of the TSH α-chain and K101 close to the C-terminus of the β-chain suggests close proximity of the termini. **D** Crosslink to K45 of the TSH α-chain are not met by any homology model of the TSHR-ECD/TSH complex. **E** Homology models suggest a potential TSHR-specific contact between E34 of the ECD to K101 of the TSH β-chain. A direct contact is observed in two homology models of the TSHR-ECD/TSH complex (one selected model depicted) supporting the feasibility of a contribution to specific TSH binding. **F** Superposition of the TSHR-LRR domain (white, PDB: 2xwt) at the C-terminal region with the FSHR-ECD/FSH complex (PDB: 4ay9). The reduced curvature of the TSHR-LRR results in an increased distance to the hormone in the N-terminal part of the TSHR template. **G** Distances between the crosslinked residues K45 of the GPH α-chain and T66 in the ECD to which the hormone is bound (green lines) and to the ECD of the adjacent ECD/hormone complex (red lines).

Downloaded from http://www.jbc.org/ at Vanderbilt University - Biomedical & Science/Engineering Libraries on November 7, 2016

FIGURE 4. Double mutant studies of the TSHR. Gs-signaling of the TSHR and variants in the absence and presence of bTSH. The S281C+I486C and S281D+I486D double mutants do not show ligand induced cAMP accumulation (**A**). In the case of the S281C+I486C double mutant, the transition to an activated receptor conformation is most likely hindered by a disulfide bond introduced between the two residues. The radioligand binding assay of the TSHR and variants (**B**) shows that the S281C+I486C variant is still capable of ligand binding suggesting that the missing ligand induced receptor activation is caused by a disruption of the activation process.

FIGURE 5. Structural variability at the ECD/TMD interface in homology models of the TSHR. The Superposition of the best scoring homology models of the largest clusters for the TSHR-ECD (**A**) and the TSHR-TMD (**B**). The ECD models are structurally similar at the putative TMD interface located at the terminal α-Helix excluding the connecting loop (depicted in orange), which was removed prior to docking. The models of the TMD, in contrast, show greater variations in the putative interface at the extracellular loops (ECL1 – light orange, ECL2 – yellow, ECL3 - white).

FIGURE 6. Evaluation of docking results by interface score and S281/I486 Cβ-distance. Two areas (black rectangles) in the plot of interface score (dG separated) versus Cβ–distance between S281 and I486 (**A**) were selected for reconstruction of the connecting loop. The best scoring models (dG separated < -6) with a S281/I486 Cβ-distance below 10 Å (**B**) show a broad variety of ECD/TMD orientation with a few clusters of similar orientations (up to 4 structures). Structures scoring significantly better (dG separated < -9) with a S281/I486 Cβ-distance between 10 and 15 Å (**C**) display a funnel at a S281/I486 Cβ–distance of 12.5 Å with almost all models displaying a similar ECD/TMD orientation.

FIGURE 7. Full-length models of the TSHR. A The best scoring full-length TSHR model of cluster one after remodeling of the connecting loop between ECD and TMD shows an almost upright orientation of the ECD towards the membrane. **B** The conformation of ECL1 includes an extended transmembrane helix 3 in the largest cluster with I486 facing away from the interface with the ECD, resulting in an increased S281/I486 Cβ –distance. **C** In the best model of cluster four only a small helical fragment is retained within the loop, resulting in closer proximity of S281 and I486. T490 is located in the extended TM3 and might influence the putative transition between the extended TM3 and the loop conformation of this region during receptor activation.

FIGURE 8. Analysis of full-length receptor models after reconstruction of the connecting loop. Comparison of the score versus Cβ-distance of S281 and I486 after clustering (**A**) shows that the best models based on score and cluster size display a S281/I486 Cβ-distance above 10 Å. Differences in contact maps (**B**) of cluster one and four (blue – contact in every model of cluster one and in none of cluster four, red – contact only in cluster four) for the S281/ECL1 interface showing that the S281/I486 contact is only observed in cluster four (upper black rectangle) and the aromatic environment of S281 including Y481and Y279 is only observed in cluster one (lower black rectangle). Superposition of the best scoring structure of cluster four (green) and the β2-adrenergic receptor (white – PDB: 2rh1) with the side-chains of the WXFG-motif depicted (**C**) shows that ECL1 of the homology model adopts a similar loop conformation in this region.

Downloaded from http://www.jbc.org/ at Vanderbilt University - Biomedical & Science/Engineering Libraries on November 7, 2016

TABLE 1

ID	1st Residue	2nd Residue	1st Sequence	2nd Sequence	cross-linker	MSMS	Δm ppm	MH+ exp	MH+ theo	cutoff distance
1	T104r	K129r	VTHIEIRD*TR	ELPLLK	DST	y3b,y4b,y7a,y6a	9.69	2065.109	2065.129	16.8
2	K51a	T111r	SKKTMLVPKD*ITSEATBBVAK	NTR	DST	b8a,y15a,y18,ab2b	9.4	2870.379	2870.406	16.8
3	K45a	T66r	KTmLVPK	TIPSHAFSD*LPNISR	DST	b5b,b4b,b11a,b4a,y4a	7.96	2600.36	2600.339	16.8
4	K45a	K91a	KTMLVPK	ATVmGNVRVENHTEBHBSTBYYHKS	DST	y2a,b6b,b21a,y15a	0.72	3985.779	3985.776	20.4
5	F1a	K101b	{FPDGEFTmQGBPEBK	BNTDYSDBIHEAIK	DST	y4a,y2a,b2b,y6a,b8b,y7a,y5a	3.81	3657.408	3657.422	17.9
6	K44a	K45a	SKKTMLVPK		BS3	b3,y2,y1,y6y3,b3	0.24	1173.722	1173.721	25.4
7	Y37a	K110b	AYPTPAR	PQK	BS3	b4a,y3a,b3a,b5a,y1b,b4a	0.14	1284.694	1284.695	26.1
8	S19a	S308r	ENKYFSK	IRGILESLMBD*ESSmQSLR	BS3	b4b,y13a,y2b,y5a	5.97	3297.63	3297.61	22.7
9	Y59b	G367r	DFmYK	{GQELK	BS3	b2a,y2b,b1b	4	1430.693	1430.687	40.9
10	Y26a	K63a	YFSKPDAPIYQBmGBBFSR	DITSEATBBVAKAFTK	BS3	b2a,b14a,b7a,b5b,b9b,b7a	2.82	4341.897	4341.909	26.1
11	K261r	K287r	ELIARNTWTLKK	ADLSYPSHBBAFK	BS3	b11a,y10b,y2a,y11a	8.18	3165.612	3165.586	25.4
12	K45a	T111r	SKK	VTHIEIRD*TR	EGS	y7a,y2b,b6a,y8a,b2a,	12.69	1826.937	1826.961	26.5
13	K67a	S298r	AFTKATVMGD*VR	NQKKIRGILESLMBD*ESSMQSLR	EGS	y7a,y3a,y4a,y6a,y9a,y8a,y5a	4.86	4244.061	4244.082	26.5
14	K44a	Y116r	AYPTPARSKK	NTRNLTYIDPDALK	EGS	b6b,b3a,y1a,y1b	8.186	2977.502	2977.527	30.8
15	K291r	S298r	NQKK	GILESLmBD*ESSmQSLRQR	BS(PEG)^{5}	y17a,b8a,y1b,y16a	2.23	3090.482	3090.475	32.1
16	K44a	Y185r	SKKTmLVPK	LYNNGFTSVQGYAFD*GTK	BS(PEG)^{5}	b8b,b2b,y7b,y1a,y1b	4.22	3330.696	3330.681	36.4
17	K63a	T111r	TMLVPKD*ITSEATBBVAKAFTK	NTR	BS(PEG)^{5}	y1a,b9a,b10a,y21a	0.28	3162.574	3162.573	32.1

***deamidated Asparagine**

Downloaded from http://www.jbc.org/ at Vanderbilt University - Biomedical & Science/Engineering Libraries on November 7, 2016

TABLE 2

Construct	Cell surface expression	cAMP basal	cAMP bTSH *(30 mU/ml)*	Spec. Const. Act	NFAT basal	NFAT bTSH *(30 mU/ml)*	Specific binding B_{Max}	Specific binding IC_{50} [nM]
wt	100.00	1.00	13.23 ± 1.19	1.00	1.00	8.26 ± 1.28	100.0	5.10 ± 1.05
S281C	70.93 ± 3.11	2.53 ± 0.21	20.45 ± 1.98	5.08 ± 0.61	0.83 ± 0.07	3.48 ± 0.46	117.5 ± 4.37	1.45 ± 0.25
S281D	25.53 ± 2.43	3.97 ± 0.44	6.92 ± 1.31	23.44 ± 2.59	1.00 ± 0.12	1.14 ± 0.14	45.3 ± 7.61	0.08 ± 0.04
S281I	51.16 ± 2.16	11.32 ± 1.13	14.26 ± 1.21	37.35 ± 5.21	0.70 ± 0.05	0.79 ± 0.05	113.5 ± 1.84	1.08 ± 0.36
I486C	23.91 ± 1.67	0.86 ± 0.19	2.70 ± 0.34	4.46 ± 0.43	1.00 ± 0.10	1.37 ± 0.04	41.0 ± 7.03	0.07 ± 0.03
I486D	34.10 ± 2.87	3.94 ± 0.39	5.51 ± 0.68	24.16 ± 1.50	0.93 ± 0.07	0.95 ± 0.06	71.0 ± 6.57	0.19 ± 0.10
I486K	23.59 ± 2.58	1.91 ± 0.25	3.51 ± 0.61	5.98 ± 1.14	0.97 ± 0.08	1.07 ± 0.02	13.8 ± 3.61	n.d.
I486S	42.75 ± 1.90	6.56 ± 0.46	15.75 ± 2.47	22.37 ± 4.02	0.82 ± 0.07	1.02 ± 0.06	104.0 ± 2.73	0.86 ± 0.30
T490C	51.82 ± 3.80	1.03 ± 0.25	11.78 ± 1.24	1.59 ± 0.13	1.01 ± 0.04	3.07 ± 0.34		
I568T	64.07 ± 3.69	13.96 ± 1.39	25.60 ± 2.91	30.19 ± 3.69	0.72 ± 0.05	2.02 ± 0.18	114.8 ± 1.26	2,23 ± 0.68
S281C+I486C	26.18 ± 1.49	1.83 ± 0.24	1.66 ± 0.24	5.79 ± 0.79	0.98 ± 0.08	1.03 ± 0.06	68.4 ± 3.55	0.11 ± 0.04
S281C+T490C	34.22 ± 2.13	1.07 ± 0.21	9.43 ± 1.39	5.57 ± 0.91	0.84 ± 0.11	1.36 ± 0.18		
S281D+I486D	31.17 ± 2.93	1.10 ± 0.23	1.42 ± 0.27	8.64 ± 1.08	1.14 ± 0.09	1.42 ± 0.11	38.5 ± 6.67	0.16 ± 0.12
S281D+I486K	22.63 ± 2.63	1.03 ± 0.15	2.12 ± 0.27	4.27 ± 0.38	1.08 ± 0.09	1.40 ± 0.14	5.4 ± 1.59	n.d.
S281I+I486S	28.14 ± 1.47	3.14 ± 0.46	4.75 ± 0.48	19.50 ± 2.96	0.66 ± 0.06	0.67 ± 0.07	33.1 ± 3.38	0.10 ± 0.03
S281I+I568T	26.83 ± 1.66	12.21 ± 1.53	11.50 ± 1.32	78.35 ± 9.64	0.67 ± 0.12	1.09 ± 0.21	77.6 ± 1.96	0.11 ± 0.06
pcDNA	7.21 ± 0.82	0.51 ± 0.10	0.46 ± 0.14		0.18 ± 0.03	0.19 ± 0.01		

Downloaded from http://www.jbc.org/ at Vanderbilt University - Biomedical & Science/Engineering Libraries on November 7, 2016

FIGURE 1

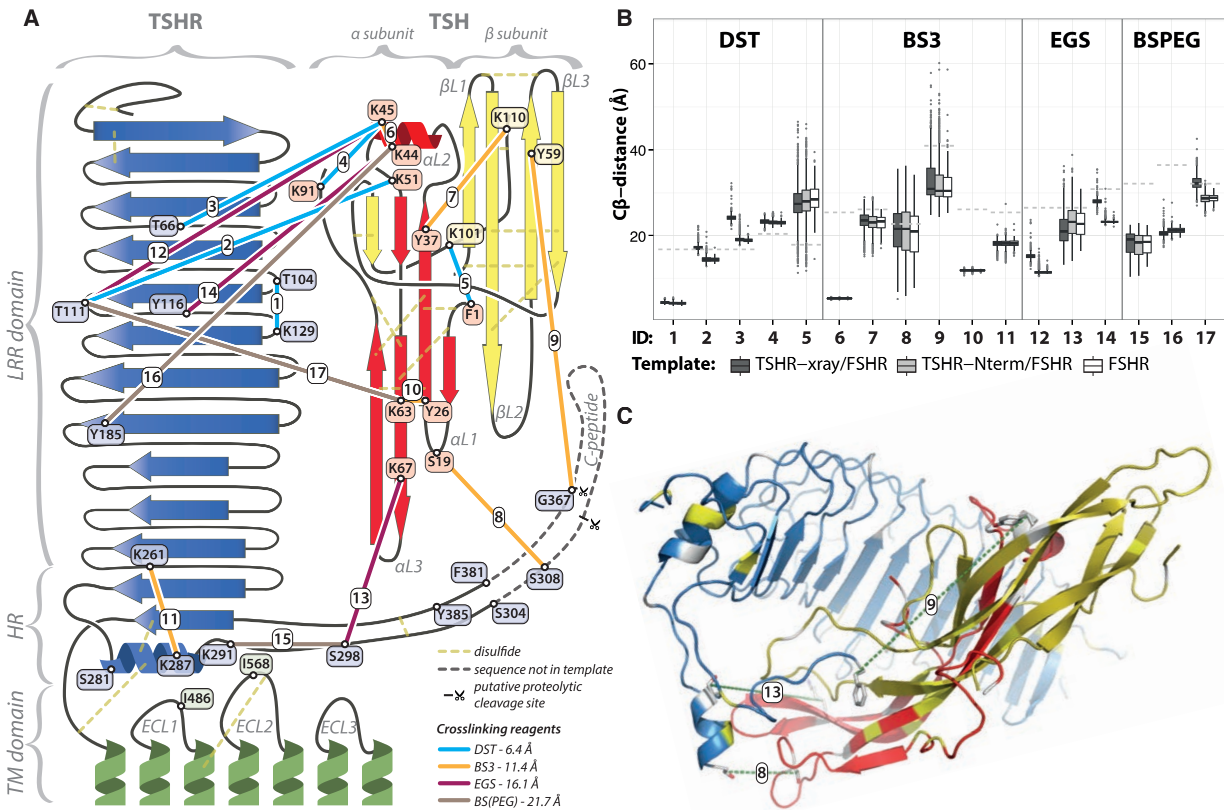

Downloaded from http://www.jbc.org/ at Vanderbilt University - Biomedical & Science/Engineering Libraries on November 7, 2016

FIGURE 2

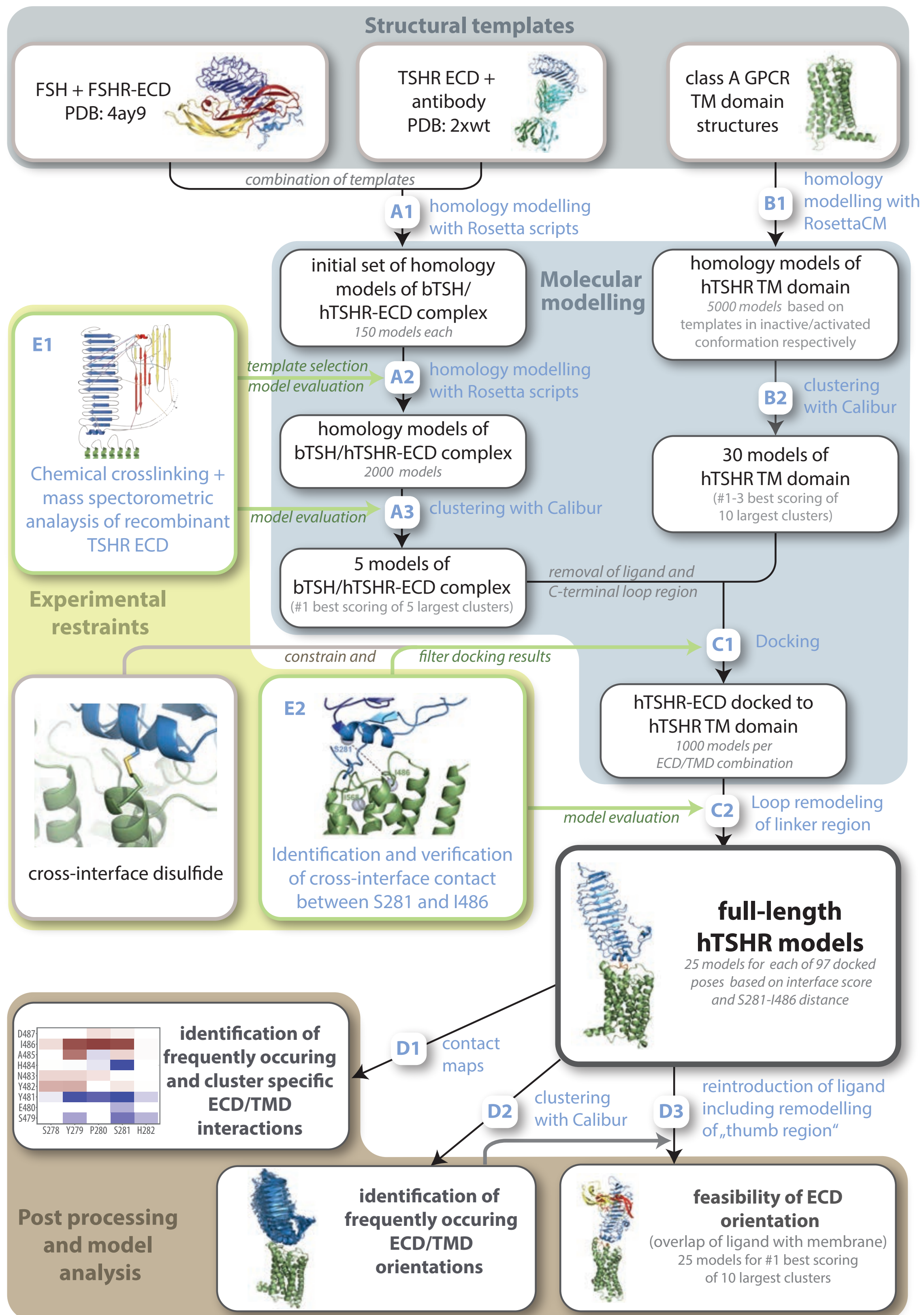

Downloaded from http://www.jbc.org/ at Vanderbilt University - Biomedical & Science/Engineering Libraries on November 7, 2016

FIGURE 3

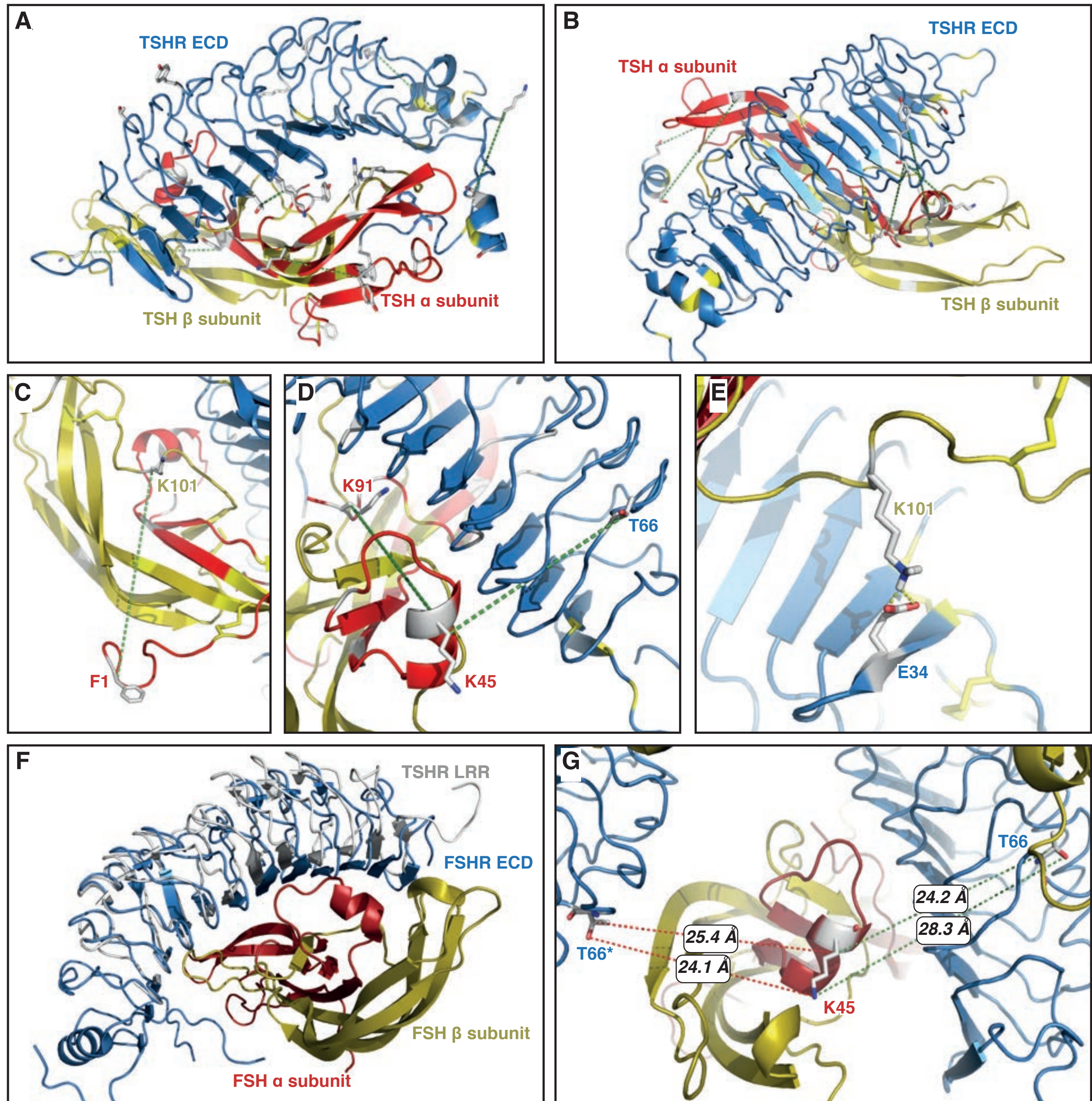

Downloaded from http://www.jbc.org/ at Vanderbilt University - Biomedical & Science/Engineering Libraries on November 7, 2016

FIGURE 4

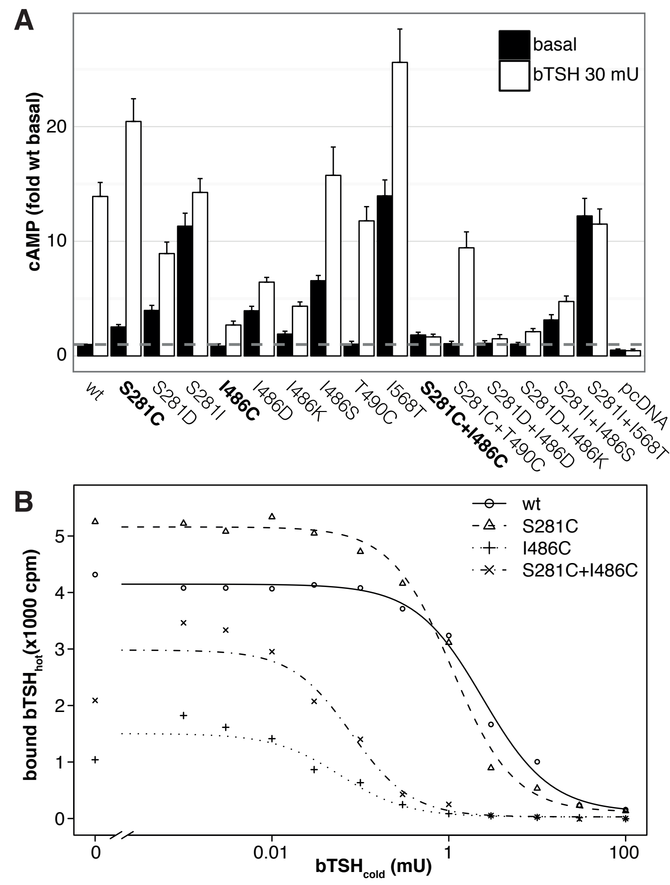

Downloaded from http://www.jbc.org/ at Vanderbilt University - Biomedical & Science/Engineering Libraries on November 7, 2016

FIGURE 5

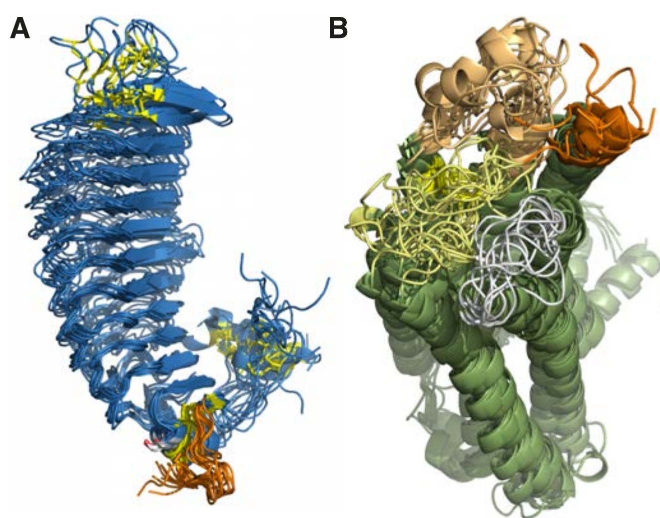

Downloaded from http://www.jbc.org/ at Vanderbilt University - Biomedical & Science/Engineering Libraries on November 7, 2016

FIGURE 6

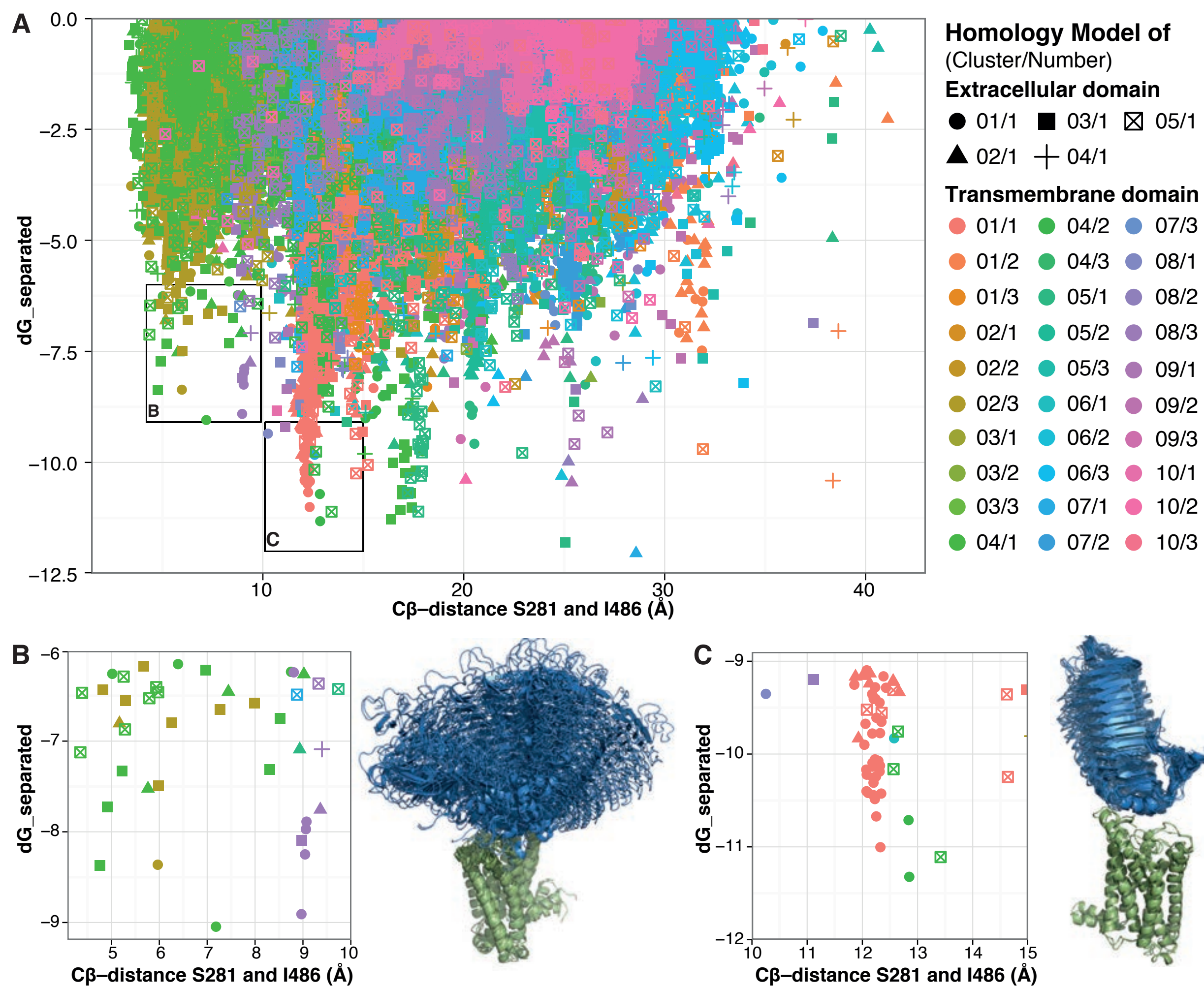

Downloaded from http://www.jbc.org/ at Vanderbilt University - Biomedical & Science/Engineering Libraries on November 7, 2016

FIGURE 7

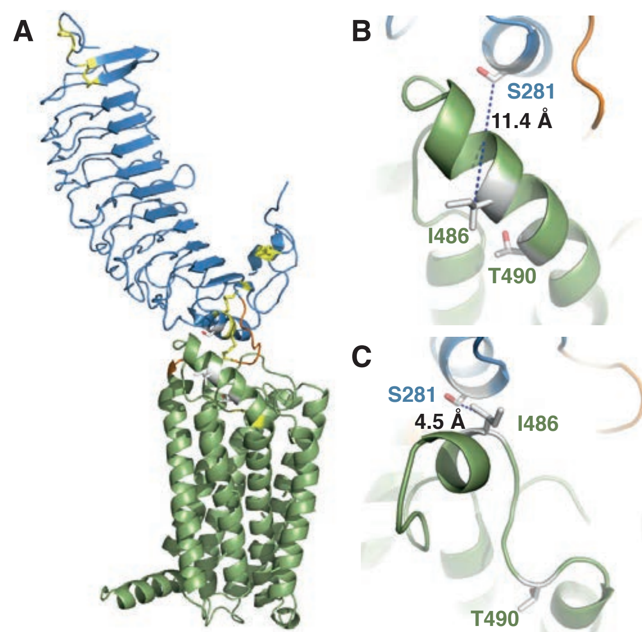

Downloaded from http://www.jbc.org/ at Vanderbilt University - Biomedical & Science/Engineering Libraries on November 7, 2016

FIGURE 8

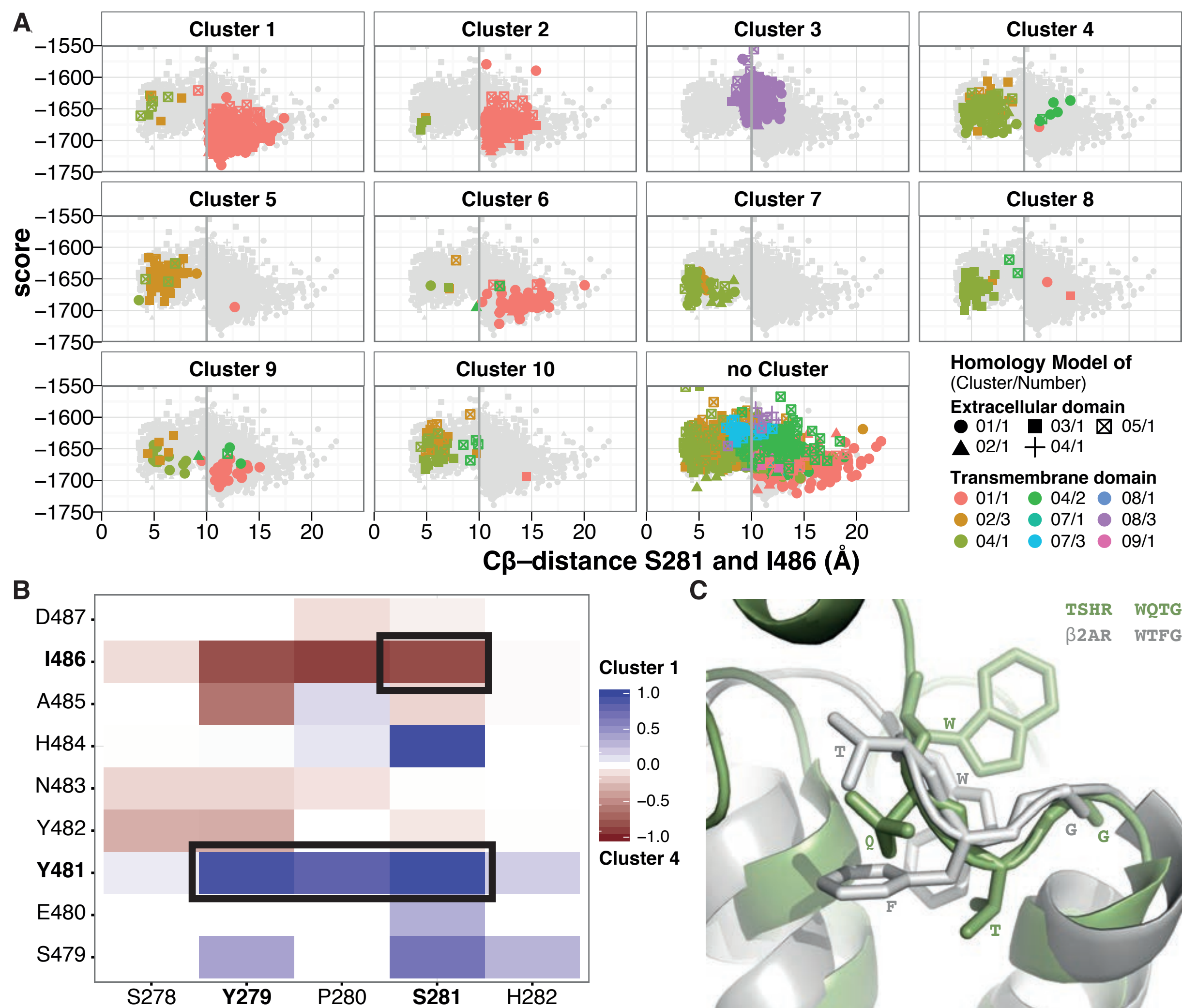

Downloaded from http://www.jbc.org/ at Vanderbilt University - Biomedical & Science/Engineering Libraries on November 7, 2016

Rearrangement of the extracellular domain/extracellular loop 1 interface is critical for thyrotropin receptor activation

Joerg Schaarschmidt, Marcus B. M. Nagel, Sandra Huth, Holger Jaeschke, Rocco Moretti, Vera Hintze, Martin von Bergen, Stefan Kalkhof, Jens Meiler and Ralf Paschke

J. Biol. Chem. published online April 26, 2016

Access the most updated version of this article at doi: 10.1074/jbc.M115.709659

Alerts:

- When this article is cited
- When a correction for this article is posted

Click here to choose from all of JBC's e-mail alerts

Supplemental material:
http://www.jbc.org/content/suppl/2016/06/01/M115.709659.DC1.html

This article cites 0 references, 0 of which can be accessed free at
http://www.jbc.org/content/early/2016/04/26/jbc.M115.709659.full.html#ref-list-1

Downloaded from http://www.jbc.org/ at Vanderbilt University - Biomedical & Science/Engineering Libraries on November 7, 2016